

Gravitational Lensing by Transparent Janis-Newman-Winicour Naked Singularities

Deyou Chen^{a,b,*}, Yiqian Chen^{c,†}, Peng Wang^{c,‡}, Tianshu Wu^{c,§} and Houwen Wu^{c,d,¶}

^a*School of Science, Xihua University, Chengdu, 610039, China*

^b*Key Laboratory of High Performance Scientific Computation,
Xihua University, Chengdu, 610039, China*

^c*Center for Theoretical Physics, College of Physics,
Sichuan University, Chengdu, 610064, China and*

^d*Department of Applied Mathematics and Theoretical Physics,
University of Cambridge, Wilberforce Road, Cambridge, CB3 0WA, UK*

The Janis-Newman-Winicour (JNW) spacetime can describe a naked singularity with a photon sphere that smoothly transforms into a Schwarzschild black hole. Our analysis reveals that photons, upon entering the photon sphere, converge to the singularity in a finite coordinate time. Furthermore, if the singularity is subjected to some regularization, these photons can traverse the regularized singularity. Subsequently, we investigate the gravitational lensing of distant sources and show that new images emerge within the critical curve formed by light rays escaping from the photon sphere. These newfound images offer a powerful tool for the detection and study of JNW naked singularities.

* deyouchen@hotmail.com

† yqchen@stu.scu.edu.cn

‡ pengw@scu.edu.cn

§ wutianshu@stu.scu.edu.cn

¶ hw598@damtp.cam.ac.uk

CONTENTS

I. Introduction	2
II. Janis-Newman-Winicour Spacetime	4
A. Metric	4
B. Null Geodesics	5
C. Regularized Naked Singularity	7
III. Lensing Images	10
IV. Point-like Source	14
A. Images Outside the Critical Curve	15
B. Images Inside the Critical Curve	16
V. Conclusions	18
Acknowledgments	19
References	19

I. INTRODUCTION

Gravitational lensing, which involves the bending of light in curved space as predicted by general relativity [1–3], is an intriguing and fundamental phenomenon with significant importance in astrophysics and cosmology. Over the past decades, extensive research has been dedicated to studying gravitational lensing, contributing significantly to addressing crucial topics, including the distribution of structures [4–6], dark matter [7–9], dark energy [10–13], quasars [14–17] and gravitational waves [18–20]. In the context of an idealized lens model featuring a distant source and a Schwarzschild black hole, the slight deflection of light in a weak gravitational field results in the observation of primary and secondary images. Moreover, strong gravitational lensing near the photon sphere gives rise to an infinite sequence of higher-order images, referred to as relativistic images, on both sides of the optic axis [21]. Notably, relativistic images exhibit minimal sensitivity to the characteristics of the astronomical source, making them valuable tools for exploring the nature of black hole spacetime.

The Event Horizon Telescope collaboration has recently achieved high angular resolution [22–35], allowing for the study of gravitational lensing in the strong gravity regime and reigniting interest in the shadow of black hole images and the associated phenomenon of strong gravitational lensing [36–76]. This research has shown a close relationship between strong gravitational lensing and bound photon orbits, which lead to the existence of photon spheres in spherically symmetric black holes. Interestingly, horizonless ultra-compact objects have been discovered to possess photon spheres, effectively mimicking black holes in various observational simulations [75, 77–86]. Future observations may offer the opportunity to test observable effects characteristic of specific spacetimes, thus enabling a precise distinction between black hole mimickers.

Among black hole mimickers, naked singularities have attracted considerable attention. Although the cosmic censorship conjecture prohibits the formation of naked singularities, they can arise through the gravitational collapse of massive objects under specific initial conditions [87–93]. Since photon spheres allow naked singularities to mimic the optical appearance of black holes, extensive research has focused on investigating the gravitational lensing phenomena associated with naked singularities [94–102]. Specifically, a photon emanating from the singularity might necessitate an infinite coordinate time to reach a distant observer, akin to photons departing from a black hole’s event horizon [103]. This discovery, coupled with the presence of photon spheres, leads to the absence of images of distant sources within the critical curve, casting a shadow in naked singularity images. Nonetheless, in certain spacetimes with naked singularities, photons can reach and escape the singularity in a finite coordinate time [103]. In such scenarios, images of naked singularities captured by distant observers hinge on the singularity’s nature, yielding distinctions from black hole images.

By minimally extending the Einstein field equations to include a massless scalar field, the Janis-Newman-Winicour (JNW) solution naturally emerges as the sole spherically symmetric solution permitted by the theory [104]. It encompasses the Schwarzschild black hole as a specific limit, excluding the existence of other spherically symmetric spacetimes featuring a regular event horizon. While the literature contains several studies on the optical characteristics of the JNW spacetime, including analyses of gravitational lensing, relativistic images, accretion and shadows [94–96, 105–112], it has seldom been explored whether photons can reach and depart from the singularity in a finite coordinate time. If this occurs, how does the singularity’s nature influence the observational signatures of JNW naked singularities?

To tackle these questions, we investigate the behavior of null geodesics around the singularity and the gravitational lensing effects on distant sources for the JNW naked singularity spacetime

in this paper. The subsequent sections of this paper are organized as follows: Section II offers a concise overview of the JNW solution and examines the behavior of photon trajectories near the singularity. In Section III, we proceed with numerically simulating images of a distant light source and a luminous celestial sphere. Following that, Section IV analyzes images produced by a point-like source. Lastly, our conclusions are presented in Section V. Throughout the paper, we adopt the convention $G = c = 1$.

II. JANIS-NEWMAN-WINICOUR SPACETIME

In this section, we provide a succinct overview of the JNW spacetime and investigate the behavior of null geodesics within it, particularly in proximity to the singularity. Subsequently, we explore light rays in regularized singularity models, wherein the singularity is substituted with a non-zero-sized regular core.

A. Metric

The JNW metric presents a static solution in Einstein-massless-scalar-field models, characterized by equations of motion,

$$\begin{aligned} R_{\mu\nu} - \frac{1}{2}Rg_{\mu\nu} &= 8\pi T_{\mu\nu}, \\ T_{\mu\nu} &= \nabla_\mu\Phi\nabla_\nu\Phi - \frac{1}{2}g_{\mu\nu}g^{\rho\sigma}\nabla_\rho\Phi\nabla_\sigma\Phi, \\ \nabla_\mu\nabla^\mu\Phi &= 0, \end{aligned} \tag{1}$$

where Φ stands for the massless scalar field, and $T_{\mu\nu}$ is the corresponding energy-momentum tensor. The metric was initially derived by Janis, Newman and Winicour, and is given as [104, 113]

$$ds^2 = -A(r)dt^2 + B(r)dr^2 + C(r)(d\theta^2 + \sin^2\theta d\varphi^2), \tag{2}$$

where the metric functions are

$$A(r) = B^{-1}(r) = \left(1 - \frac{r_g}{r}\right)^\gamma \text{ and } C(r) = \left(1 - \frac{r_g}{r}\right)^{1-\gamma} r^2. \tag{3}$$

In addition, the scalar field is expressed as

$$\Phi = \frac{q}{r_g} \ln\left(1 - \frac{r_g}{r}\right), \tag{4}$$

where q is the scalar charge.

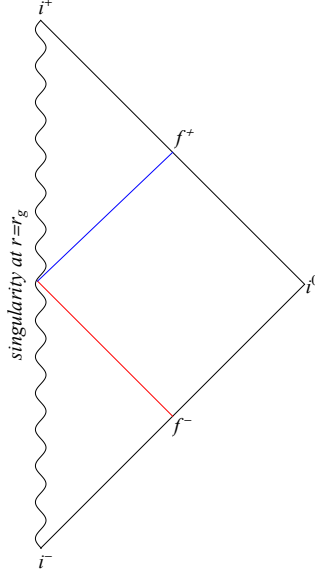


FIG. 1. Penrose diagram for JNW naked singularity. The red and blue lines denote light rays travelling toward and away from the singularity, respectively.

The JNW metric is characterized by two parameters, γ and r_g , which are related to the ADM mass M and the scalar charge q by [104]

$$\gamma = \frac{2M}{r_g} \text{ and } r_g = 2\sqrt{M^2 + q^2}. \quad (5)$$

When $\gamma = 1$, the JNW metric describes Schwarzschild black holes with no scalar charge. For $0.5 < \gamma < 1$, the JNW metric represents weakly naked singularity solutions with a non-trivial scalar field profile. In this case, a naked curvature singularity occurs at $r = r_g$, and a photon sphere is present at $r_{ps} = r_g(1 + 2\gamma)/2$. However, the photon sphere disappears in the JNW metric when $0 \leq \gamma < 0.5$, leading to distinct light propagations. Since a spacetime with photon spheres can mimic black hole observations, such as black hole shadows, the focus in this paper is on the JNW metric with $0.5 < \gamma < 1$. The causal structure of the JNW naked singularity is depicted in the corresponding Penrose diagram shown in FIG. 1. The timelike curvature singularity is located at $r = r_g$.

B. Null Geodesics

For a photon with 4-momentum vector $p^\mu = (\dot{t}, \dot{r}, \dot{\theta}, \dot{\varphi})$, where dots stand for derivative with respect to some affine parameter λ , the null geodesic equations exhibit separability and can be

fully characterized by three conserved quantities,

$$E = p_\mu \partial_t^\mu = -p_t, \quad L_z = p_\mu \partial_\varphi^\mu = p_\varphi, \quad L^2 = K^{\mu\nu} p_\mu p_\nu = p_\theta^2 + L_z^2 \csc^2 \theta, \quad (6)$$

where the tensor $K^{\mu\nu}$ is a symmetric Killing tensor

$$K = C^2(r) (d\theta \otimes d\theta + \sin^2 \theta d\varphi \otimes d\varphi). \quad (7)$$

Here, E , L_z and L denote the total energy, the angular momentum parallel to the axis of symmetry, and the total angular momentum, respectively. Consequently, the 4-momentum $p = p_\mu dx^\mu$ can be expressed in terms of E , L_z and L as follows

$$p = -E dt \pm_r \sqrt{\mathcal{R}(r)} dr \pm_\theta \sqrt{\Theta(\theta)} d\theta + L d\varphi, \\ \mathcal{R}(r) = B(r) \left[\frac{E^2}{A(r)} - \frac{L^2}{C(r)} \right] \text{ and } \Theta(\theta) = L^2 - L_z^2 \csc^2 \theta, \quad (8)$$

where the choices of sign \pm_r and \pm_θ depend on the radial and polar directions of travel, respectively.

The null geodesic equations can then be written as

$$\dot{t} = \frac{E}{A(r)}, \quad \dot{r} = \pm_r L \sqrt{b^{-2} - V_{\text{eff}}(r)}, \quad \dot{\theta} = \pm_\theta \frac{\sqrt{L^2 - L_z^2 \csc^2 \theta}}{C(r)}, \quad \dot{\varphi} = \frac{L_z}{C(r) \sin^2 \theta}, \quad (9)$$

where $b \equiv L/E$ is the impact parameter, and the effective potential of photons is defined as

$$V_{\text{eff}}(r) = \frac{A(r)}{C(r)}. \quad (10)$$

Particularly, the rate of change of radius r with respect to time t can be expressed as

$$\frac{dr}{dt} = \pm A(r) \sqrt{1 - b^2 V_{\text{eff}}(r)}. \quad (11)$$

The plus and minus signs in the equation represent motion radially outward and inward towards the naked singularity, respectively. It is crucial to note that null geodesics are only permitted when $b^{-2} \geq V_{\text{eff}}(r)$. The maximum of $V_{\text{eff}}(r)$ determines the locations of circular light rays, which constitute the photon sphere. Interestingly, when the impact parameter b is smaller than the critical parameter b_c (representing the impact parameter for photon trajectories on the photon sphere), photons can cross the photon sphere and travel toward the singularity.

To investigate whether a photon can reach and leave the singularity at $r = r_g$ within a finite coordinate time (i.e., the proper time measured by a distant observer), we first consider a radial light ray with $b = 0$, arriving at or departing from the singularity at $t = 0$. For this light ray, eqn. (11) yields

$$t(r) = \pm \frac{r_g^\gamma (r - r_g)^{1-\gamma}}{\gamma - 1} {}_2F_1 \left(1 - \gamma, -\gamma, 2 - \gamma, 1 - \frac{r}{r_g} \right), \quad (12)$$

where plus and minus signs correspond to the outgoing and ingoing cases, respectively. Here, ${}_2F_1(a, b, c; x)$ denotes the hypergeometric function. The implication of eqn. (12) is twofold: firstly, photons emitted from distant sources reach the singularity in a finite coordinate time, and secondly, photons leaving the singularity reach distant observers in a finite coordinate time. It is worth mentioning that $t(r)$ approaches infinity in the limit of $\gamma = 1$, which is consistent with expectations for Schwarzschild black holes. For general null geodesics, eqn. (11) describes the behavior of photons around the singularity at $r = r_g$, yielding

$$\frac{dt}{dr} = \pm r_g^\gamma (r - r_g)^{-\gamma} + \mathcal{O}\left((r - r_g)^{1-\gamma}\right). \quad (13)$$

The corresponding asymptotic solution is

$$t(r) \sim \pm \frac{r_g^\gamma (r - r_g)^{1-\gamma}}{1 - \gamma}, \quad (14)$$

which also shows that photons travel through the singularity in a finite coordinate time.

Furthermore, in the vicinity of the singularity, the solutions of the null geodesic equations (9) take the form

$$\begin{aligned} r(\lambda) &= r_g \pm_r E\lambda + \mathcal{O}\left(|\lambda|^{\frac{1}{2-2\gamma}}\right), \\ t(\lambda) &= t_0 \pm_r \frac{E^{1-\gamma} r_g^\gamma |\lambda|^{1-\gamma}}{1 - \gamma} + \mathcal{O}\left(|\lambda|^{1-\gamma}\right), \\ \theta(\lambda) &= \theta_0 \pm_\theta \sqrt{L^2 - L_z^2} \csc^2 \theta_0 \frac{E^{\gamma-1} |\lambda|^\gamma}{\gamma r_g^{1+\lambda}} + \mathcal{O}\left(|\lambda|^\gamma\right), \\ \varphi(\lambda) &= \varphi_0 + \frac{L_z E^{\gamma-1} \csc^2 \theta_0 |\lambda|^\gamma}{\gamma r_g^{\gamma+1}} + \mathcal{O}\left(|\lambda|^\gamma\right), \end{aligned} \quad (15)$$

where t_0 , θ_0 and φ_0 are the integration constants, and we assume $r(0) = r_g$. It shows the existence of two classes of light rays: radially outgoing and ingoing light rays, denoted as $+_r$ and $-_r$, respectively. To simplify, we adopt $\lambda < 0$ for ingoing light rays and $\lambda > 0$ for outgoing ones. As the affine parameter λ approaches 0 from the right and left, respectively, both outgoing and ingoing light rays converge towards the singularity. In FIG. 1, the blue and red lines represent outgoing and ingoing light rays, respectively.

C. Regularized Naked Singularity

As mentioned earlier, photons with a sufficiently small impact parameter can reach the singularity in a finite coordinate time, prompting inquiry into their fate at the singularity as observed by

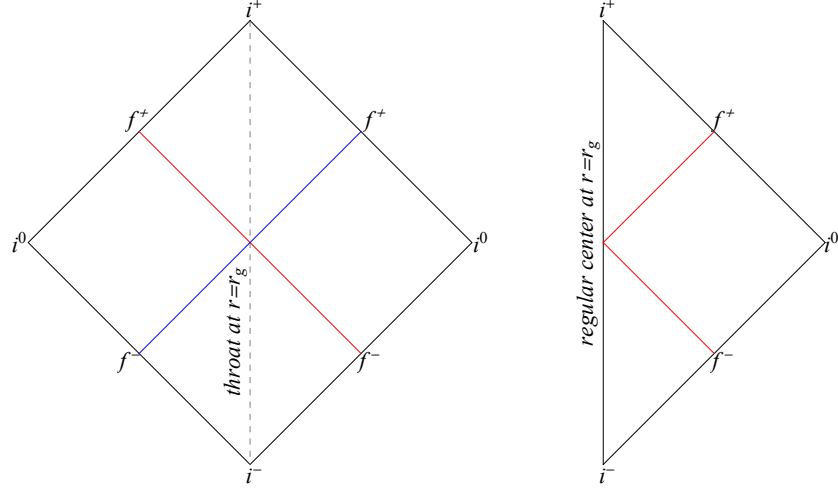


FIG. 2. Penrose diagram for regularized JNW naked singularity with a wormhole throat (**Left**) and a regular center (**Right**).

distant observers. However, the existence of the singularity indicates a breakdown in the applicability of general relativity around it, which has ignited the pursuit of a theory of quantum gravity. Given the lack of a definitive quantum gravity framework, researchers frequently resort to effective models to regularize such singularities, thereby facilitating investigations into the characteristics of null geodesics at these points. These effective models often employ a regularized singularity metric that can describe spacetime like wormholes or non-singular manifolds. An example in the former category is the modified JNW geometry through the application of the Simpson and Visser (SV) method [114]. Specifically, the SV-modified JNW geometry is derived by substituting r with $\sqrt{r^2 + \epsilon^2}$, where ϵ represents the SV parameter. When two such SV-modified JNW metrics are connected by a thin shell at $r = r_g$, the resulting spacetime forms a traversable wormhole with a throat located at $r = r_g$. The corresponding Penrose diagram is depicted in the left panel of FIG. 2, where the red and blue lines illustrate that light rays moving toward $r = r_g$ will traverse the throat and enter another universe.

Of particular interest, the regularization of singularities can be achieved by incorporating higher-order curvature terms, such as the complete α' corrections of string theory [115–117]. This approach leads to a regularized singularity spacetime that maintains regularity throughout, and $r = r_g$ serves as the center of this well-behaved manifold. Moreover, apart from a vicinity around the center, the singularity spacetime closely approximates the regularized singularity spacetime. Therefore, photons with sufficiently small impact parameters are able to traverse the neighborhood of the center and reach distant observers. The right panel of FIG. 2 shows the corresponding Penrose

diagram, where a red line illustrates a light ray passing through the neighborhood of the center. Note that this light ray comprises both radially outgoing and ingoing branches. Typically, a specific formulation of the regularized singularity spacetime is necessary to establish the connection between the ingoing and outgoing branches.

For the sake of simplicity, we construct a regularized singularity spacetime by matching the JNW metric with a regular spacetime, introducing a thin shell centered at $r = r_g$ with a tiny yet non-zero radius ϵ . The metric of the regular spacetime within this thin shell is described by

$$ds_{\text{in}}^2 = -A_{\text{in}}(r) dt^2 + B_{\text{in}}(r) dr^2 + C_{\text{in}}(r) (d\theta^2 + \sin^2 \theta d\varphi^2). \quad (16)$$

In the vicinity of $r = r_g$, the metric functions are expanded in the following manner,

$$\begin{aligned} A_{\text{in}}(r) &= a_0 + a_1 (r - r_g) + \cdots, \\ B_{\text{in}}(r) &= b_0 + b_1 (r - r_g) + \cdots, \\ C_{\text{in}}(r) &= (r - r_g)^2 [c_0 + c_1 (r - r_g) + \cdots], \end{aligned} \quad (17)$$

where the equality of b_0 and c_0 arises from the absence of a conical singularity at $r = r_g$. For a light ray entering the regular core from the JNW spacetime, the corresponding energy E_{in} and angular momentum L_{in} in the regular core are related to the energy E and angular momentum L in the JNW spacetime as [118, 119],

$$E_{\text{in}} = \sqrt{\frac{A_{\text{in}}(r_g + \epsilon)}{A(r_g + \epsilon)}} E \text{ and } L_{\text{in}} = \sqrt{\frac{C_{\text{in}}(r_g + \epsilon)}{C(r_g + \epsilon)}} L. \quad (18)$$

Due to the spherical symmetry, we restrict the light ray to the equatorial plane and assume its entry and exit from the thin shell occur at $\varphi = \varphi_1$ and φ_2 , respectively. Beyond the thin shell, in the JNW spacetime, the light ray follows the trajectory given by eqn. (15), encompassing both ingoing and outgoing branches that terminates at $\varphi = \varphi_1$ and departs from $\varphi = \varphi_2$ on the thin shell, respectively. The deflection angle $\Delta\varphi = \varphi_2 - \varphi_1$, due to the influence of the regular core, is quantified as

$$\Delta\varphi = 2 \int_{b_{\text{in}}}^{r_g + \epsilon} \frac{\sqrt{A_{\text{in}}(r) B_{\text{in}}(r)} dr}{C_{\text{in}}(r) \sqrt{b_{\text{in}}^{-2} - A_{\text{in}}(r) / C_{\text{in}}(r)}}, \quad (19)$$

where $b_{\text{in}} = L_{\text{in}} / E_{\text{in}}$. As ϵ approaches zero,

$$\Delta\varphi \rightarrow 2 \arccos \left(\epsilon^{\gamma-1/2} r_g^{-\gamma-1/2} b \right) \rightarrow \pi, \quad (20)$$

illustrating that the entry and exit points on the thin shell are antipodal opposite. Furthermore, when the singularity is modeled with an infinitesimally small regular core, the portion of the light

ray within the thin shell can be safely disregarded. Thus, the light ray is well approximated by the combination of the ingoing and outgoing branches in the JNW metric outside the thin shell. Since these branches intersect with the thin shell at exactly two antipodal points, their connection is given by

$$\theta \rightarrow \pi - \theta \text{ and } \varphi \rightarrow \varphi + \pi. \quad (21)$$

In short, the condition (21) and the conservation of E , L_z and L determine the corresponding outgoing branch for a given ingoing branch.

Given its stronger theoretical motivation and its potential for generating a richer set of observational outcomes, we focus on the case of a regularized JNW singularity with a regular center throughout the remainder of this paper. Moreover, the observations related to the wormhole case can be encompassed within the context of the regular center case, an aspect that we will briefly address in the concluding section.

III. LENSING IMAGES

This section presents a numerical simulation of gravitational lensing images produced by a distant luminous object and a celestial sphere around JNW naked singularities, aiming to illustrate the gravitational lensing phenomenon. The observer and the center of the luminous object are positioned on the equatorial plane at $(r, \phi) = (10M, \pi)$ and $(25M, \pi/6)$, respectively, while the luminous celestial sphere is placed at $r = 25M$. Here, M represents the mass of the JNW metric. To generate observational images, we vary the observer's viewing angle and numerically integrate 2000×2000 photon trajectories until they intersect with the celestial sphere. For a detailed explanation of the numerical implementation, interested readers can refer to [102].

The strong deflection around the photon sphere causes light rays to produce multiple images of the distant object when they orbit the photon sphere multiple times. We conveniently classify these images based on the number of orbits, denoted by n . Moreover, the positive and negative signs of n indicate whether the orbiting occurs in the counter-clockwise or clockwise directions. As anticipated, light rays can circle around the photon sphere slightly outside of it, generating images similar to the Schwarzschild black hole case. Interestingly, our earlier discussion revealed that light rays, being able to traverse the singularities, can also orbit the photon sphere from inside, resulting in a new set of images. Throughout the remainder of this paper, we use the notations $n^>$ and $n^<$ to refer to the $|n|^{\text{th}}$ -order images produced by light rays orbiting n times outside and inside the

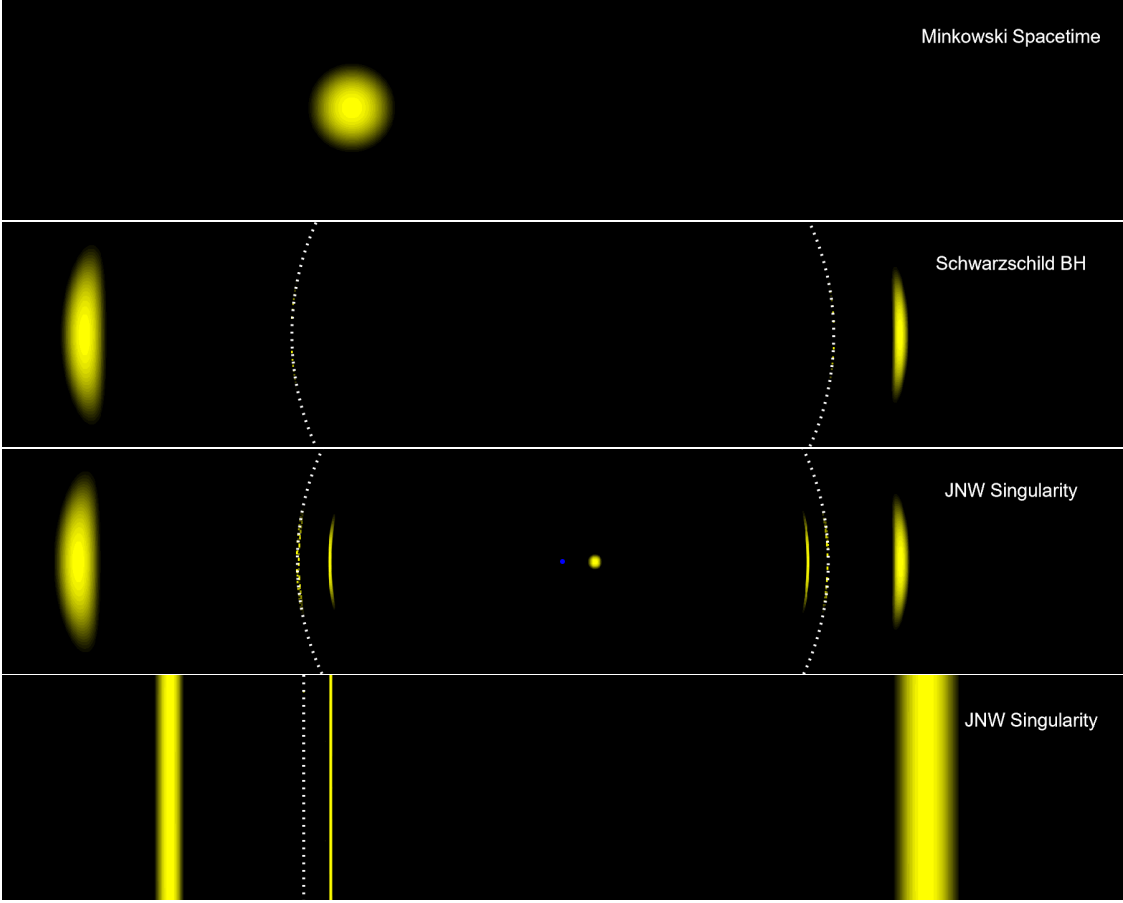


FIG. 3. Images of a luminous object centered at $x_s^\mu = (0, 25M, \pi/2, \pi/6)$ as viewed by an observer positioned at $x_o^\mu = (0, 10M, \pi/2, \pi)$ in Minkowski spacetime, a Schwarzschild black hole, and a JNW singularity with $\gamma = 2/3$. The critical curve, formed by light rays escaping from the photon sphere, is depicted with dashed white lines, while the JNW singularity is marked by a blue dot. Unlike the Schwarzschild black hole, the JNW singularity displays additional images of the object inside the critical curve, due to the capability of light rays to pass through the singularity. A zoom-in view near the JNW singularity's critical curve is presented in the bottom panel, showing one higher-order image outside the critical curve and two higher-order images inside it.

photon sphere, respectively.

FIG. 3 displays images of the luminous object in three different scenarios: Minkowski spacetime, a Schwarzschild black hole, and a JNW naked singularity with $\gamma = 2/3$. In the figure, the dashed white lines represent the critical curve, which is formed by photons originating from the photon sphere. The images produced by light rays with $n^>$ and $n^<$ lie outside and inside the critical curve, respectively. Outside the critical curve, both the Schwarzschild black hole and the JNW singularity cases exhibit two observable images: $n = +0^>$ and $-0^>$, referred to as the primary and

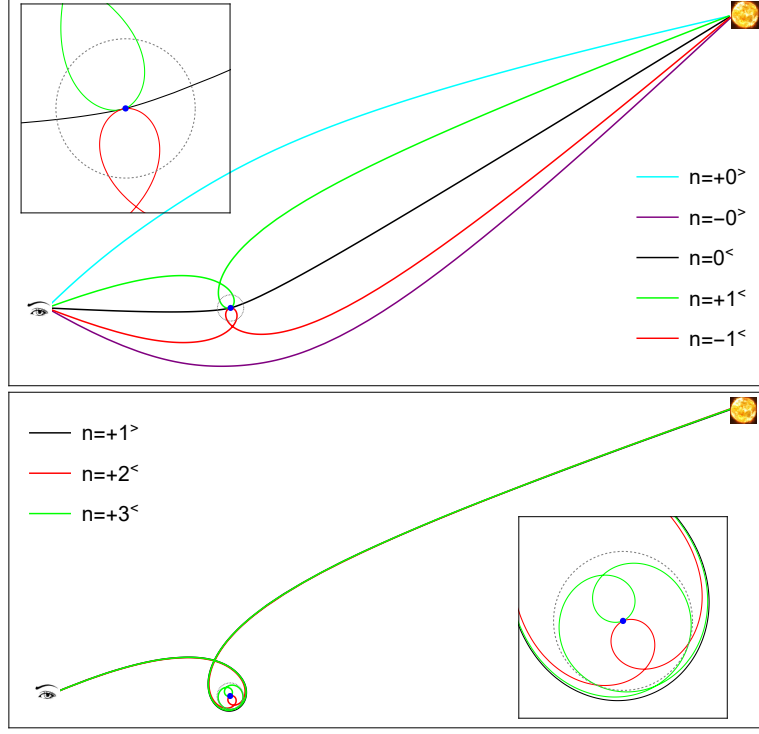


FIG. 4. **Upper:** Light rays responsible for generating the object images in the third panel (located just above the bottom panel) of FIG. 3, where the images with $n = +0^>$, $+1^<$, $0^<$, $-1^<$ and $-0^>$ are presented from left to right. **Lower:** Light rays that produce the object images in the bottom panel of FIG. 3, where the images with $n = +1^>$, $+3^<$ and $+2^<$ are displayed from left to right. In n , the number denotes the number of orbits of light rays, while the $+$ and $-$ signs indicate the counter-clockwise and clockwise directions, respectively. Additionally, the $>$ and $<$ symbols correspond to orbiting outside and inside the photon sphere, respectively. The dashed circular lines represent the photon sphere.

secondary images, respectively. These images can be analyzed using the weak lensing approximation. However, for the Schwarzschild black hole, no images are visible inside the critical curve due to the presence of the event horizon. In contrast, the JNW naked singularity presents an image with $n = 0^<$ near the center and two additional images with $n = \pm 1^<$ within the critical curve. The light rays responsible for generating these images are illustrated in the upper panel of FIG. 4. It should be noted that the higher-order images are located so close to the critical curve that they cannot be resolved in the two middle panels of FIG. 3. To provide a closer view of the critical curve region, the bottom panel of FIG. 3 zooms in and displays the $n = +1^>$, $+3^<$ and $+2^<$ images from left to right. Furthermore, the light rays responsible for producing these three images are depicted in the lower panel of FIG. 4. It is worth emphasizing that, except for the $n = 0^<$ image, all other images are significantly distorted due to the effects of gravitational lensing.

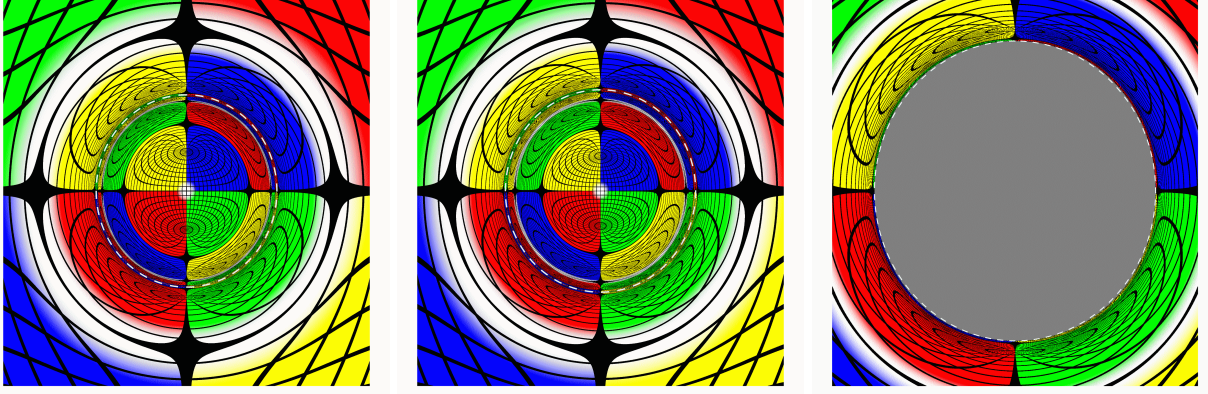


FIG. 5. Images of a celestial sphere located at $r = 25M$ in the JNW metric with $\gamma = 0.6$ (**Left**), 0.9 (**Middle**) and 1 (**Right**). The observer's location is $x_o^\mu = (0, 10M, \pi/2, \pi)$, and the field of view spans $2\pi/5$. The dashed lines represent the critical curve. In the case of $\gamma = 1$, the JNW metric corresponds to a Schwarzschild black hole, and thus, the right panel includes the black hole shadow depicted as a gray area. For $\gamma = 0.6$ and 0.9 , the image inside the critical curve is formed by light rays passing through the singularity. A central white dot is visible, surrounded by two white Einstein rings.

Furthermore, FIG. 5 illustrates images of the celestial sphere in both a Schwarzschild black hole and JNW singularities. The celestial sphere is divided into four quadrants, each distinguished by a different color, and a white dot is placed in front of the observer. Moreover, a grid of black lines, with adjacent lines separated by $\pi/18$, is overlaid to represent constant longitude and latitude. In the images shown in FIG. 5, the dashed circular lines represent the critical curve. Outside the critical curve, the celestial sphere images in JNW singularities bear a resemblance to those observed in the Schwarzschild black hole spacetime. However, while shadows are observed in the black hole image, the celestial sphere images persist within the critical curve for JNW singularities. This unique feature is attributed to the transparency of the singularity, allowing light to traverse through it.

Outside the critical curve, we observe a white Einstein ring generated by the white dot placed on the celestial sphere in both the Schwarzschild black hole and JNW singularity cases. However, in JNW singularities, an additional Einstein ring appears within the critical curve, representing photons that pass through the singularity with angular coordinate changes of $\Delta\varphi = 3\pi$. Furthermore, light rays passing through the singularity and undergoing an angular coordinate change of $\Delta\varphi = \pi$ result in a white dot positioned at the center of the image.

IV. POINT-LIKE SOURCE

In order to investigate point-source gravitational lensing, we adopt an idealized thin lens model that assumes a high degree of alignment among the source, lens and observer. The lens equation, as presented in [21, 120], is expressed as

$$\beta = \vartheta - \frac{D_{LS}}{D_{OS}} \Delta\alpha, \quad (22)$$

where β represents the angular separation between the source and the lens, ϑ denotes the angular separation between the lens and the image, and $\Delta\alpha$ represents the offset of the total deflection angle α after accounting for all the windings experienced by the photon. Here, the distances D_{OL} , D_{LS} and D_{OS} correspond to the observer-lens, lens-source and observer-source distances, respectively. Furthermore, we define the magnification μ of an image as the ratio of the image's flux to the flux of the unlensed source. This ratio is determined by the solid angles of the image and the unlensed source measured by the observer, resulting in the following expression [71, 120]

$$\mu = \mu^r \mu^t = \frac{\vartheta}{\beta} \frac{d\vartheta}{d\beta}. \quad (23)$$

In the above equation, the factors $\mu^r \equiv d\vartheta/d\beta$ and $\mu^t \equiv \vartheta/\beta$ represent the radial and tangential magnifications of the image, respectively. Additionally, the sign of the magnification factors determines the parity of the image.

By taking advantage of the spherical symmetry, our computations of the deflection angle α are confined to the equatorial plane. Within the thin-lens approximation, the deflection angle α is governed by the expression from [21],

$$\alpha = I(b) - \pi, \quad (24)$$

where $I(b)$ represents the change in φ , and b denotes the impact parameter related to ϑ through the equation $b = D_{OL}\vartheta$. When a photon approaches a turning point at $r = r_0$ and then gets deflected towards a distant observer, the integral $I(b)$ is given by

$$I(b) = 2 \int_{r_0}^{\infty} \frac{dr}{C(r) \sqrt{b^{-2} - V_{\text{eff}}(r)}}, \quad (25)$$

where r_0 is determined by $V_{\text{eff}}(r_0) = b^{-2}$. On the other hand, if the photon passes through the singularity at $r = r_g$, the azimuthal angle φ increases by π , leading to the expression,

$$I(b) = 2 \int_{r_g}^{\infty} \frac{dr}{C(r) \sqrt{b^{-2} - V_{\text{eff}}(r)}} + \pi. \quad (26)$$

γ	0.6	0.7	0.8	0.9
$\vartheta_{\pm\infty}$	± 25.1927	± 26.5221	± 27.2768	± 27.7592
$\vartheta_{+0>}$	5.4121×10^6	5.4121×10^6	5.4121×10^6	5.4121×10^6
$\Delta\vartheta_{+1>}$	3.9857×10^{-2}	3.6895×10^{-2}	3.5898×10^{-2}	3.5424×10^{-2}
$\Delta\vartheta_{+2>}$	7.4431×10^{-5}	6.8900×10^{-5}	6.7037×10^{-5}	6.6152×10^{-5}
$\Delta\vartheta_{+3>}$	1.3900×10^{-7}	1.2867×10^{-7}	1.2519×10^{-7}	1.2354×10^{-7}
$\vartheta_{-0>}$	-4.1204×10^5	-4.1204×10^5	-4.1204×10^5	-4.1204×10^5
$\Delta\vartheta_{-1>}$	-3.9853×10^{-2}	-3.6892×10^{-2}	-3.5894×10^{-2}	-3.5420×10^{-2}
$\Delta\vartheta_{-2>}$	-7.4424×10^{-5}	-6.8893×10^{-5}	-6.7031×10^{-5}	-6.6146×10^{-5}
$\Delta\vartheta_{-3>}$	-1.3898×10^{-7}	-1.2865×10^{-7}	-1.2516×10^{-7}	-1.2352×10^{-7}
$\mu_{+0>}$	1.0058	1.0058	1.0058	1.0058
$\mu_{+1>}$	1.9502×10^{-18}	1.9002×10^{-18}	1.9013×10^{-18}	1.9093×10^{-18}
$\mu_{+2>}$	3.6362×10^{-21}	3.5436×10^{-21}	3.5459×10^{-21}	3.5609×10^{-21}
$\mu_{+3>}$	6.7903×10^{-24}	6.6174×10^{-24}	6.6217×10^{-24}	6.6498×10^{-24}
$\mu_{-0>}$	-5.8297×10^{-3}	-5.8297×10^{-3}	-5.8297×10^{-3}	-5.8297×10^{-3}
$\mu_{-1>}$	-1.9502×10^{-18}	-1.9002×10^{-18}	-1.9013×10^{-18}	-1.9093×10^{-18}
$\mu_{-2>}$	-3.6362×10^{-21}	-3.5436×10^{-21}	-3.5459×10^{-21}	-3.5609×10^{-21}
$\mu_{-3>}$	-6.7903×10^{-24}	-6.6174×10^{-24}	-6.6217×10^{-24}	-6.6498×10^{-24}

TABLE I. The angular position $\vartheta_{\pm n>}$ and the magnification factor $\mu_{\pm n>}$ of images outside the critical curve for a point-like source in JNW singularities with varying γ . Here, $\Delta\vartheta_{\pm n>} \equiv \vartheta_{\pm n>} - \vartheta_{\pm\infty}$ represents the angular separation between the n^{th} -order relativistic images and the critical curve. The superscript $>$ indicates that the images are produced by light rays with $b > b_c$ and therefore reside outside the critical curve. The values $M = 4.31 \times 10^6 M_\odot$, $D_{OL} = D_{LS} = 7.86$ kpc and $\beta = 5$ arcsec are used. All angles are expressed in units of microarcseconds.

A. Images Outside the Critical Curve

As depicted above, the images located outside the critical curve are produced by light rays reaching a turning point at $r = r_0$, which lies outside the photon sphere. To calculate the angular position $\vartheta_{\pm 0>}$ and magnification factor $\mu_{\pm 0>}$ for the primary image with $n = +0>$ and the secondary one with $n = -0>$, we employ eqn. (25) to numerically determine $I(b)$ and $dI(b)/db$. By utilizing the resulting $I(b)$ and $dI(b)/db$, eqns. (22) and (23) provide the desired $\vartheta_{\pm 0>}$ and $\mu_{\pm 0>}$. Additionally, our findings reveal that $\mu_{\pm 0>}^t \sim \beta^{-1}$ and $\mu_{\pm 0>}^r \sim \mathcal{O}(1)$, as expected from weak gravitational lensing. When $\beta \ll 1$, the magnitude of $\mu_{\pm 0>}^t$ greatly exceeds that of $\mu_{\pm 0>}^r$, resulting in significantly distorted images.

In the case of relativistic images with $|n| \geq 1$, their impact parameter b closely approaches the critical impact parameter b_c , allowing us to expand $I(b)$ around $b = b_c$. In this strong deflection limit, the total deflection angle α is expressed as [121, 122]

$$\alpha = -\bar{a}^> \ln(b/b_c - 1) + \bar{b}^> + \mathcal{O}((b/b_c - 1) \ln(b/b_c - 1)), \quad (27)$$

where

$$\bar{a}^> = 1 \text{ and } \bar{b}^> = -\pi + I_R^> + \ln \left[\frac{2(2\gamma + 1)}{2\gamma - 1} \right]. \quad (28)$$

Here, the term $I_R^>$ represents a regular integral that can be computed numerically. Using eqns. (22) and (23), we can solve for the angular position $\vartheta_{\pm n>}$ and magnification factor $\mu_{\pm n>}$ of n^{th} -order relativistic images. Specifically, the angular position $\vartheta_{\pm n>}$ is given by [121]

$$\vartheta_{\pm n>} = \vartheta_{\pm n>}^0 + \frac{b_c e_n^> D_{OS}}{\bar{a}^> D_{LS} D_{OL}} (\beta - \vartheta_{\pm n>}^0), \quad (29)$$

where $e_n^> = e^{\frac{\bar{b}^> - 2\pi n}{\bar{a}^>}}$, and $\vartheta_{\pm n>}^0$, satisfying $\alpha(\vartheta_{\pm n>}^0) = \pm 2n\pi$, is given by

$$\vartheta_{\pm n>}^0 = \pm \frac{b_c}{D_{OL}} (1 + e_n^>). \quad (30)$$

The factors μ^t and μ^r are then expressed as

$$\mu_{\pm n>}^t = \pm \frac{b_c (1 + e_n^>)}{\beta D_{OL}} \text{ and } \mu_{\pm n>}^r = \frac{b_c e_n^> D_{OS}}{\bar{a}^> D_{LS} D_{OL}}, \quad (31)$$

which gives the magnification factor $\mu_{\pm n>} = \mu_{\pm n>}^r \mu_{\pm n>}^t$. As $|\mu_{\pm n>}^t| \gg |\mu_{\pm n>}^r|$, the relativistic images are significantly stretched along the critical curve.

To numerically estimate $\vartheta_{\pm n>}$ and $\mu_{\pm n>}$ in an astrophysical setting, we model the supermassive black hole Sgr A* located at the center of our Galaxy as a JNW singularity. Specifically, we assume a mass of $M = 4.31 \times 10^6 M_\odot$ and a lens-source distance of $D_{OL} = 7.86$ kpc. Additionally, a source is positioned at $D_{LS} = 7.86$ kpc with an angular separation of $\beta = 5$ arcsec. Table I presents $\vartheta_{\pm 0>}$ and $\mu_{\pm 0>}$ for the primary and secondary images, along with $\Delta\vartheta_{\pm n>} \equiv \vartheta_{\pm n>} - \vartheta_{\pm \infty}$ and $\mu_{\pm n>}$ for the relativistic images, considering various values of γ in JNW singularities. Here, $\vartheta_{\pm \infty} = \lim_{n \rightarrow \infty} \vartheta_{\pm n>}^0 = \pm b_c / D_{OL}$ represents the angular position of the critical curve. The results indicate that the angular position $\vartheta_{\pm n>}$ and magnification factor $\mu_{\pm n>}$ of the images outside the critical curve show little sensitivity to γ .

B. Images Inside the Critical Curve

When $b < b_c$, photons emitted from the source have the capability to traverse the singularity, resulting in additional images within the critical curve. In this scenario, the deflection angle α is

γ	0.6	0.7	0.8	0.9
$\vartheta_{\pm\infty}$	± 25.1927	± 26.5221	± 27.2768	± 27.7592
$\vartheta_{0<}$	-2.6208×10^{-4}	-2.6208×10^{-4}	-2.6208×10^{-4}	-2.6208×10^{-4}
$\Delta\vartheta_{+1<}$	-11.5719	-9.6609	-8.3838	-7.4221
$\Delta\vartheta_{+2<}$	-1.2227	-8.0648×10^{-1}	-6.1750×10^{-1}	-5.0363×10^{-1}
$\Delta\vartheta_{+3<}$	-5.6756×10^{-2}	-3.6433×10^{-2}	-2.7577×10^{-2}	-2.2344×10^{-2}
$\Delta\vartheta_{-1<}$	11.5724	9.6614	8.3843	7.4225
$\Delta\vartheta_{-2<}$	1.2228	8.0655×10^{-1}	6.1756×10^{-1}	5.0368×10^{-1}
$\Delta\vartheta_{-3<}$	5.6761×10^{-2}	3.6436×10^{-2}	2.7580×10^{-2}	2.2346×10^{-2}
$\mu_{0<}$	2.7475×10^{-21}	2.7475×10^{-21}	2.7475×10^{-21}	2.7475×10^{-21}
$\mu_{+1<}$	-6.3652×10^{-17}	-8.2124×10^{-17}	-9.0031×10^{-17}	-9.2892×10^{-17}
$\mu_{+2<}$	-2.6383×10^{-17}	-1.9202×10^{-17}	-1.5425×10^{-17}	-1.2950×10^{-17}
$\mu_{+3<}$	-1.3787×10^{-18}	-9.3375×10^{-19}	-7.2756×10^{-19}	-6.0023×10^{-19}
$\mu_{-1<}$	6.3652×10^{-17}	8.2124×10^{-17}	9.0031×10^{-17}	9.2892×10^{-17}
$\mu_{-2<}$	2.6383×10^{-17}	1.9202×10^{-17}	1.5425×10^{-17}	1.2950×10^{-17}
$\mu_{-3<}$	1.3787×10^{-18}	9.3375×10^{-19}	7.2756×10^{-19}	6.0023×10^{-19}

TABLE II. The angular position $\vartheta_{\pm n<}$ and the magnification factor $\mu_{\pm n<}$ of images inside the critical curve for a point-like source in JNW singularities with varying γ . The parameters M , D_{OL} , D_{LS} and β are chosen to be consistent with those presented in Table I. All angles are expressed in units of microarcseconds.

computed using eqn. (26). For light rays that pass through the singularity without orbiting it, their impact parameter b is often much smaller than b_c , leading to

$$\alpha \simeq 2b \int_{r_g}^{\infty} \frac{dr}{C(r)} = \frac{b}{M}. \quad (32)$$

Consequently, the resulting image with $n = 0<$ has

$$\vartheta_{0<} \simeq -\frac{D_{OS}M}{D_{LS}D_{OL}}\beta \text{ and } \mu_{0<}^r = \mu_{0<}^t \simeq -\frac{D_{OS}M}{D_{LS}D_{OL}}, \quad (33)$$

where we assume $M \ll D_{LS}D_{OL}/D_{OS}$. Notably, the $n = 0<$ image is barely distorted by gravitational lensing since $\mu_{0<}^r = \mu_{0<}^t$.

Relativistic images produced by light rays traversing the singularity have been discussed in a generic spherically symmetric metric using the strong deflection approximation [102]. Applying these calculations to the JNW singularity, we obtain

$$\alpha = -\bar{a}^< \ln(b^2/b_c^2 - 1) + \bar{b}^< + \mathcal{O}((b^2/b_c^2 - 1) \ln(b^2/b_c^2 - 1)), \quad (34)$$

where

$$\bar{a}^< = 2 \text{ and } \bar{b}^< = 2 \ln \left[\frac{4(2\gamma + 1)}{2\gamma - 1} \right] + I_R^<.$$

As a result, the angular position of the n^{th} -order images is given by

$$\vartheta_{\pm n}^< = \vartheta_{\pm n}^0 - \frac{b_c e_n^< D_{OS}}{2\bar{a}^< D_{LS} D_{OL}} \frac{(\beta - \vartheta_{\pm n}^0)}{(1 + e_n^<)^{3/2}}, \quad (35)$$

where

$$\vartheta_{\pm n}^0 = \pm \frac{b_c}{D_{OL}} \frac{1}{\sqrt{1 + e_n^<}} \text{ and } e_n^< = e^{\frac{\bar{b}^< - 2\pi n}{\bar{a}^<}}. \quad (36)$$

The corresponding radial and tangential magnification factors are

$$\mu_{\pm n}^r = -\frac{b_c e_n^< D_{OS}}{2\bar{a}^< D_{OL} D_{LS}} (1 + e_n^<)^{2/3} \text{ and } \mu_{\pm n}^t = \pm \frac{b_c}{\beta D_{OL} \sqrt{1 + e_n^<}}, \quad (37)$$

respectively, showing that the relativistic images are highly stretched along the critical curve.

Similarly, in the aforementioned astrophysical scenario, Table II presents the angular position and magnification factor of the images inside the critical curve. For the $n = 0^<$ image, its angular position and magnification factor hardly depend on γ . It shows that the $n = 0^<$ image is almost centered in the image plane, positioned far away from the critical curve. Moreover, compared to the relativistic images listed in the table, the $n = 0^<$ image has a smaller magnification factor, mainly due to the very small value of $\mu_{0^<}^t$. Notably, the relativistic images inside the critical curve are more widely separated and magnified compared to the images outside the critical curve, resulting from the significant bending of light rays upon entering or exiting the photon sphere. This bending also leads to a noticeable dependence of the angular positions and magnification factors on γ . As γ increases, the relativistic images tend to approach the critical curve. Additionally, there is a marked rise (fall) in the magnification factor of the $n = \pm 1^<$ ($n = \pm 2^<$ and $\pm 3^<$) images with the increase of γ .

V. CONCLUSIONS

This paper investigated the phenomenon of gravitational lensing by JNW naked singularities, which possess a photon sphere. Similar to Schwarzschild black holes, light rays that orbit the photon sphere outside of it result in multiple images of a distant source beyond the critical curve. However, when photons originating from the source enter the photon sphere, they are observed to approach the singularity in a finite coordinate time. Assuming that the singularity is remedied by

a regular core, these photons can traverse the regularized singularity, leading to the emergence of new images inside the critical curve. In particular, the $n = 0^<$ image, formed by light rays passing directly through the singularity, remains well-separated from the critical curve and exhibits minimal distortion. Furthermore, we have demonstrated that relativistic images inside the critical curve are more magnified and positioned farther from the critical curve than those outside the critical curve, enhancing the possibility of resolving relativistic images within the critical curve. As a result, these findings present a powerful means of detecting and studying JNW naked singularities through their distinct gravitational lensing signatures.

Although current observational facilities lack the capability to distinguish new images within the critical curve in JNW singularity spacetime, the next-generation Very Long Baseline Interferometry has emerged as a promising tool for this purpose [123–125]. Hence, it would be highly intriguing to extend our analysis to encompass more astrophysically realistic models, such as the rotating JNW naked singularity solution and the imaging of accretion disks around JNW singularities.

Lastly, it is important to note that the optical appearances of distant sources within the JNW singularity spacetime are contingent upon the specific regularization method applied to address the singularity. In cases where the singularity is regularized by a wormhole throat instead of a regular core, photons reaching the throat will traverse to another universe. In scenarios where the source and observer inhabit the same universe, the resultant images are solely located outside the critical curve, bearing a close resemblance to the black hole case. In contrast, if the source and the observer reside in different universes, only images situated within the critical curve become observable, thereby presenting observational phenomena distinct from those associated with black holes.

ACKNOWLEDGMENTS

We are grateful to Qingyu Gan and Xin Jiang for useful discussions and valuable comments. This work is supported in part by NSFC (Grant No. 12105191, 12275183, 12275184 and 11875196). Houwen Wu is supported by the International Visiting Program for Excellent Young Scholars of Sichuan University.

-
- [1] F. W. Dyson, A. S. Eddington, and C. Davidson. A Determination of the Deflection of Light by the Sun's Gravitational Field, from Observations Made at the Total Eclipse of May 29, 1919. *Phil. Trans.*

- Roy. Soc. Lond. A*, 220:291–333, 1920. [doi:10.1098/rsta.1920.0009](#). I
- [2] Albert Einstein. Lens-Like Action of a Star by the Deviation of Light in the Gravitational Field. *Science*, 84:506–507, 1936. [doi:10.1126/science.84.2188.506](#).
- [3] A. Eddington. *SPACE, TIME AND GRAVITATION. AN OUTLINE OF THE GENERAL RELATIVITY THEORY*. 1987. I
- [4] Yannick Mellier. Probing the universe with weak lensing. *Ann. Rev. Astron. Astrophys.*, 37:127–189, 1999. [arXiv:astro-ph/9812172](#), [doi:10.1146/annurev.astro.37.1.127](#). I
- [5] Matthias Bartelmann and Peter Schneider. Weak gravitational lensing. *Phys. Rept.*, 340:291–472, 2001. [arXiv:astro-ph/9912508](#), [doi:10.1016/S0370-1573\(00\)00082-X](#).
- [6] Catherine Heymans et al. CFHTLenS tomographic weak lensing cosmological parameter constraints: Mitigating the impact of intrinsic galaxy alignments. *Mon. Not. Roy. Astron. Soc.*, 432:2433, 2013. [arXiv:1303.1808](#), [doi:10.1093/mnras/stt601](#). I
- [7] Nick Kaiser and Gordon Squires. Mapping the dark matter with weak gravitational lensing. *Astrophys. J.*, 404:441–450, 1993. [doi:10.1086/172297](#). I
- [8] Douglas Clowe, Marusa Bradac, Anthony H. Gonzalez, Maxim Markevitch, Scott W. Randall, Christine Jones, and Dennis Zaritsky. A direct empirical proof of the existence of dark matter. *Astrophys. J. Lett.*, 648:L109–L113, 2006. [arXiv:astro-ph/0608407](#), [doi:10.1086/508162](#).
- [9] Farruh Atamurotov, Ahmadjon Abdujabbarov, and Wen-Biao Han. Effect of plasma on gravitational lensing by a Schwarzschild black hole immersed in perfect fluid dark matter. *Phys. Rev. D*, 104(8):084015, 2021. [doi:10.1103/PhysRevD.104.084015](#). I
- [10] Marek Biesiada. Strong lensing systems as a probe of dark energy in the universe. *Phys. Rev. D*, 73:023006, 2006. [doi:10.1103/PhysRevD.73.023006](#). I
- [11] Shuo Cao, Marek Biesiada, Rapha Gavazzi, Aleksandra Piórkowska, and Zong-Hong Zhu. Cosmology With Strong-lensing Systems. *Astrophys. J.*, 806:185, 2015. [arXiv:1509.07649](#), [doi:10.1088/0004-637X/806/2/185](#).
- [12] T. M. C. Abbott et al. Dark Energy Survey Year 1 Results: Cosmological constraints from cluster abundances and weak lensing. *Phys. Rev. D*, 102(2):023509, 2020. [arXiv:2002.11124](#), [doi:10.1103/PhysRevD.102.023509](#).
- [13] T. M. C. Abbott et al. Dark Energy Survey Year 3 results: Cosmological constraints from galaxy clustering and weak lensing. *Phys. Rev. D*, 105(2):023520, 2022. [arXiv:2105.13549](#), [doi:10.1103/PhysRevD.105.023520](#). I
- [14] Xiaohui Fan et al. The Discovery of a luminous $z = 5.80$ quasar from the Sloan Digital Sky Survey. *Astron. J.*, 120:1167–1174, 2000. [arXiv:astro-ph/0005414](#), [doi:10.1086/301534](#). I
- [15] Chien Y. Peng, Chris D. Impey, Hans-Walter Rix, Christopher S. Kochanek, Charles R. Keeton, Emilio E. Falco, Joseph Lehar, and Brian A. McLeod. Probing the coevolution of supermassive black holes and galaxies using gravitationally lensed quasar hosts. *Astrophys. J.*, 649:616–634, 2006. [arXiv:astro-ph/0603248](#), [doi:10.1086/506266](#).

- [16] Masamune Oguri and Philip J. Marshall. Gravitationally lensed quasars and supernovae in future wide-field optical imaging surveys. *Mon. Not. Roy. Astron. Soc.*, 405:2579–2593, 2010. [arXiv:1001.2037](#), [doi:10.1111/j.1365-2966.2010.16639.x](#).
- [17] Minghao Yue, Xiaohui Fan, Jinyi Yang, and Feige Wang. Revisiting the Lensed Fraction of High-redshift Quasars. *Astrophys. J.*, 925(2):169, 2022. [arXiv:2112.02821](#), [doi:10.3847/1538-4357/ac409b](#). I
- [18] Uros Seljak and Christopher M. Hirata. Gravitational lensing as a contaminant of the gravity wave signal in CMB. *Phys. Rev. D*, 69:043005, 2004. [arXiv:astro-ph/0310163](#), [doi:10.1103/PhysRevD.69.043005](#). I
- [19] Jose M. Diego, Tom Broadhurst, and George Smoot. Evidence for lensing of gravitational waves from LIGO-Virgo data. *Phys. Rev. D*, 104(10):103529, 2021. [arXiv:2106.06545](#), [doi:10.1103/PhysRevD.104.103529](#).
- [20] Andreas Finke, Stefano Foffa, Francesco Iacovelli, Michele Maggiore, and Michele Mancarella. Probing modified gravitational wave propagation with strongly lensed coalescing binaries. *Phys. Rev. D*, 104(8):084057, 2021. [arXiv:2107.05046](#), [doi:10.1103/PhysRevD.104.084057](#). I
- [21] K. S. Virbhadra and George F. R. Ellis. Schwarzschild black hole lensing. *Phys. Rev. D*, 62:084003, 2000. [arXiv:astro-ph/9904193](#), [doi:10.1103/PhysRevD.62.084003](#). I, IV, IV
- [22] Kazunori Akiyama et al. First M87 Event Horizon Telescope Results. I. The Shadow of the Supermassive Black Hole. *Astrophys. J. Lett.*, 875:L1, 2019. [arXiv:1906.11238](#), [doi:10.3847/2041-8213/ab0ec7](#). I
- [23] Kazunori Akiyama et al. First M87 Event Horizon Telescope Results. II. Array and Instrumentation. *Astrophys. J. Lett.*, 875(1):L2, 2019. [arXiv:1906.11239](#), [doi:10.3847/2041-8213/ab0c96](#).
- [24] Kazunori Akiyama et al. First M87 Event Horizon Telescope Results. III. Data Processing and Calibration. *Astrophys. J. Lett.*, 875(1):L3, 2019. [arXiv:1906.11240](#), [doi:10.3847/2041-8213/ab0c57](#).
- [25] Kazunori Akiyama et al. First M87 Event Horizon Telescope Results. IV. Imaging the Central Supermassive Black Hole. *Astrophys. J. Lett.*, 875(1):L4, 2019. [arXiv:1906.11241](#), [doi:10.3847/2041-8213/ab0e85](#).
- [26] Kazunori Akiyama et al. First M87 Event Horizon Telescope Results. V. Physical Origin of the Asymmetric Ring. *Astrophys. J. Lett.*, 875(1):L5, 2019. [arXiv:1906.11242](#), [doi:10.3847/2041-8213/ab0f43](#).
- [27] Kazunori Akiyama et al. First M87 Event Horizon Telescope Results. VI. The Shadow and Mass of the Central Black Hole. *Astrophys. J. Lett.*, 875(1):L6, 2019. [arXiv:1906.11243](#), [doi:10.3847/2041-8213/ab1141](#).
- [28] Kazunori Akiyama et al. First M87 Event Horizon Telescope Results. VII. Polarization of the Ring. *Astrophys. J. Lett.*, 910(1):L12, 2021. [arXiv:2105.01169](#), [doi:10.3847/2041-8213/abe71d](#).
- [29] Kazunori Akiyama et al. First M87 Event Horizon Telescope Results. VIII. Magnetic Field Structure

- near The Event Horizon. *Astrophys. J. Lett.*, 910(1):L13, 2021. [arXiv:2105.01173](#), [doi:10.3847/2041-8213/abe4de](#).
- [30] Kazunori Akiyama et al. First Sagittarius A* Event Horizon Telescope Results. I. The Shadow of the Supermassive Black Hole in the Center of the Milky Way. *Astrophys. J. Lett.*, 930(2):L12, 2022. [doi:10.3847/2041-8213/ac6674](#).
 - [31] Kazunori Akiyama et al. First Sagittarius A* Event Horizon Telescope Results. II. EHT and Multiwavelength Observations, Data Processing, and Calibration. *Astrophys. J. Lett.*, 930(2):L13, 2022. [doi:10.3847/2041-8213/ac6675](#).
 - [32] Kazunori Akiyama et al. First Sagittarius A* Event Horizon Telescope Results. III. Imaging of the Galactic Center Supermassive Black Hole. *Astrophys. J. Lett.*, 930(2):L14, 2022. [doi:10.3847/2041-8213/ac6429](#).
 - [33] Kazunori Akiyama et al. First Sagittarius A* Event Horizon Telescope Results. IV. Variability, Morphology, and Black Hole Mass. *Astrophys. J. Lett.*, 930(2):L15, 2022. [doi:10.3847/2041-8213/ac6736](#).
 - [34] Kazunori Akiyama et al. First Sagittarius A* Event Horizon Telescope Results. V. Testing Astrophysical Models of the Galactic Center Black Hole. *Astrophys. J. Lett.*, 930(2):L16, 2022. [doi:10.3847/2041-8213/ac6672](#).
 - [35] Kazunori Akiyama et al. First Sagittarius A* Event Horizon Telescope Results. VI. Testing the Black Hole Metric. *Astrophys. J. Lett.*, 930(2):L17, 2022. [doi:10.3847/2041-8213/ac6756](#). I
 - [36] Heino Falcke, Fulvio Melia, and Eric Agol. Viewing the shadow of the black hole at the galactic center. *Astrophys. J. Lett.*, 528:L13, 2000. [arXiv:astro-ph/9912263](#), [doi:10.1086/312423](#). I
 - [37] Clarissa-Marie Claudel, K. S. Virbhadra, and G. F. R. Ellis. The Geometry of photon surfaces. *J. Math. Phys.*, 42:818–838, 2001. [arXiv:gr-qc/0005050](#), [doi:10.1063/1.1308507](#).
 - [38] Ernesto F. Eiroa, Gustavo E. Romero, and Diego F. Torres. Reissner-Nordstrom black hole lensing. *Phys. Rev. D*, 66:024010, 2002. [arXiv:gr-qc/0203049](#), [doi:10.1103/PhysRevD.66.024010](#).
 - [39] K. S. Virbhadra. Relativistic images of Schwarzschild black hole lensing. *Phys. Rev. D*, 79:083004, 2009. [arXiv:0810.2109](#), [doi:10.1103/PhysRevD.79.083004](#).
 - [40] Akifumi Yumoto, Daisuke Nitta, Takeshi Chiba, and Naoshi Sugiyama. Shadows of Multi-Black Holes: Analytic Exploration. *Phys. Rev. D*, 86:103001, 2012. [arXiv:1208.0635](#), [doi:10.1103/PhysRevD.86.103001](#).
 - [41] Shao-Wen Wei and Yu-Xiao Liu. Observing the shadow of Einstein-Maxwell-Dilaton-Axion black hole. *JCAP*, 11:063, 2013. [arXiv:1311.4251](#), [doi:10.1088/1475-7516/2013/11/063](#).
 - [42] Alexander F. Zakharov. Constraints on a charge in the Reissner-Nordström metric for the black hole at the Galactic Center. *Phys. Rev. D*, 90(6):062007, 2014. [arXiv:1407.7457](#), [doi:10.1103/PhysRevD.90.062007](#).
 - [43] Farruh Atamurotov, Sushant G. Ghosh, and Bobomurat Ahmedov. Horizon structure of rotating Einstein–Born–Infeld black holes and shadow. *Eur. Phys. J. C*, 76(5):273, 2016. [arXiv:1506.03690](#),

- [doi:10.1140/epjc/s10052-016-4122-9](https://doi.org/10.1140/epjc/s10052-016-4122-9).
- [44] Sara Dastan, Reza Saffari, and Saheb Soroushfar. Shadow of a Kerr-Sen dilaton-axion Black Hole. 10 2016. [arXiv:1610.09477](https://arxiv.org/abs/1610.09477).
 - [45] Pedro V. P. Cunha, Carlos A. R. Herdeiro, Burkhard Kleihaus, Jutta Kunz, and Eugen Radu. Shadows of Einstein–dilaton–Gauss–Bonnet black holes. *Phys. Lett. B*, 768:373–379, 2017. [arXiv:1701.00079](https://arxiv.org/abs/1701.00079), [doi:10.1016/j.physletb.2017.03.020](https://doi.org/10.1016/j.physletb.2017.03.020).
 - [46] Mingzhi Wang, Songbai Chen, and Jiliang Jing. Shadow casted by a Konoplya-Zhidenko rotating non-Kerr black hole. *JCAP*, 10:051, 2017. [arXiv:1707.09451](https://arxiv.org/abs/1707.09451), [doi:10.1088/1475-7516/2017/10/051](https://doi.org/10.1088/1475-7516/2017/10/051).
 - [47] Muhammed Amir, Balendra Pratap Singh, and Sushant G. Ghosh. Shadows of rotating five-dimensional charged EMCS black holes. *Eur. Phys. J. C*, 78(5):399, 2018. [arXiv:1707.09521](https://arxiv.org/abs/1707.09521), [doi:10.1140/epjc/s10052-018-5872-3](https://doi.org/10.1140/epjc/s10052-018-5872-3).
 - [48] Ali Övgün, İzzet Sakallı, and Joel Saavedra. Shadow cast and Deflection angle of Kerr-Newman-Kasuya spacetime. *JCAP*, 10:041, 2018. [arXiv:1807.00388](https://arxiv.org/abs/1807.00388), [doi:10.1088/1475-7516/2018/10/041](https://doi.org/10.1088/1475-7516/2018/10/041).
 - [49] Volker Perlick, Oleg Yu. Tsupko, and Gennady S. Bisnovatyi-Kogan. Black hole shadow in an expanding universe with a cosmological constant. *Phys. Rev. D*, 97(10):104062, 2018. [arXiv:1804.04898](https://arxiv.org/abs/1804.04898), [doi:10.1103/PhysRevD.97.104062](https://doi.org/10.1103/PhysRevD.97.104062).
 - [50] Tao Zhu, Qiang Wu, Mubasher Jamil, and Kimet Jusufi. Shadows and deflection angle of charged and slowly rotating black holes in Einstein-Æther theory. *Phys. Rev. D*, 100(4):044055, 2019. [arXiv:1906.05673](https://arxiv.org/abs/1906.05673), [doi:10.1103/PhysRevD.100.044055](https://doi.org/10.1103/PhysRevD.100.044055).
 - [51] Cosimo Bambi, Katherine Freese, Sunny Vagnozzi, and Luca Visinelli. Testing the rotational nature of the supermassive object M87* from the circularity and size of its first image. *Phys. Rev. D*, 100(4):044057, 2019. [arXiv:1904.12983](https://arxiv.org/abs/1904.12983), [doi:10.1103/PhysRevD.100.044057](https://doi.org/10.1103/PhysRevD.100.044057).
 - [52] Akash K. Mishra, Sumanta Chakraborty, and Sudipta Sarkar. Understanding photon sphere and black hole shadow in dynamically evolving spacetimes. *Phys. Rev. D*, 99(10):104080, 2019. [arXiv:1903.06376](https://arxiv.org/abs/1903.06376), [doi:10.1103/PhysRevD.99.104080](https://doi.org/10.1103/PhysRevD.99.104080).
 - [53] Sunny Vagnozzi and Luca Visinelli. Hunting for extra dimensions in the shadow of M87*. *Phys. Rev. D*, 100(2):024020, 2019. [arXiv:1905.12421](https://arxiv.org/abs/1905.12421), [doi:10.1103/PhysRevD.100.024020](https://doi.org/10.1103/PhysRevD.100.024020).
 - [54] Rahul Kumar, Sushant G. Ghosh, and Anzhong Wang. Shadow cast and deflection of light by charged rotating regular black holes. *Phys. Rev. D*, 100(12):124024, 2019. [arXiv:1912.05154](https://arxiv.org/abs/1912.05154), [doi:10.1103/PhysRevD.100.124024](https://doi.org/10.1103/PhysRevD.100.124024).
 - [55] Liang Ma and H. Lu. Bounds on photon spheres and shadows of charged black holes in Einstein-Gauss-Bonnet-Maxwell gravity. *Phys. Lett. B*, 807:135535, 2020. [arXiv:1912.05569](https://arxiv.org/abs/1912.05569), [doi:10.1016/j.physletb.2020.135535](https://doi.org/10.1016/j.physletb.2020.135535).
 - [56] Alireza Allahyari, Mohsen Khodadi, Sunny Vagnozzi, and David F. Mota. Magnetically charged black holes from non-linear electrodynamics and the Event Horizon Telescope. *JCAP*, 02:003, 2020. [arXiv:1912.08231](https://arxiv.org/abs/1912.08231), [doi:10.1088/1475-7516/2020/02/003](https://doi.org/10.1088/1475-7516/2020/02/003).
 - [57] Xiao-Xiong Zeng, Hai-Qing Zhang, and Hongbao Zhang. Shadows and photon spheres with spherical

- accretions in the four-dimensional Gauss–Bonnet black hole. *Eur. Phys. J. C*, 80(9):872, 2020. [arXiv:2004.12074](#), [doi:10.1140/epjc/s10052-020-08449-y](#).
- [58] Xiao-Xiong Zeng and Hai-Qing Zhang. Influence of quintessence dark energy on the shadow of black hole. *Eur. Phys. J. C*, 80(11):1058, 2020. [arXiv:2007.06333](#), [doi:10.1140/epjc/s10052-020-08656-7](#).
- [59] Rittick Roy and Sayan Chakrabarti. Study on black hole shadows in asymptotically de Sitter space-times. *Phys. Rev. D*, 102(2):024059, 2020. [arXiv:2003.14107](#), [doi:10.1103/PhysRevD.102.024059](#).
- [60] Peng-Cheng Li, Minyong Guo, and Bin Chen. Shadow of a Spinning Black Hole in an Expanding Universe. *Phys. Rev. D*, 101(8):084041, 2020. [arXiv:2001.04231](#), [doi:10.1103/PhysRevD.101.084041](#).
- [61] Rahul Kumar, Sushant G. Ghosh, and Anzhong Wang. Gravitational deflection of light and shadow cast by rotating Kalb-Ramond black holes. *Phys. Rev. D*, 101(10):104001, 2020. [arXiv:2001.00460](#), [doi:10.1103/PhysRevD.101.104001](#).
- [62] Sunny Vagnozzi, Cosimo Bambi, and Luca Visinelli. Concerns regarding the use of black hole shadows as standard rulers. *Class. Quant. Grav.*, 37(8):087001, 2020. [arXiv:2001.02986](#), [doi:10.1088/1361-6382/ab7965](#).
- [63] Mohsen Khodadi, Alireza Allahyari, Sunny Vagnozzi, and David F. Mota. Black holes with scalar hair in light of the Event Horizon Telescope. *JCAP*, 09:026, 2020. [arXiv:2005.05992](#), [doi:10.1088/1475-7516/2020/09/026](#).
- [64] Abhishek Chowdhuri and Arpan Bhattacharyya. Shadow analysis for rotating black holes in the presence of plasma for an expanding universe. 12 2020. [arXiv:2012.12914](#).
- [65] K. Saurabh and Kimet Jusufi. Imprints of dark matter on black hole shadows using spherical accretions. *Eur. Phys. J. C*, 81(6):490, 2021. [arXiv:2009.10599](#), [doi:10.1140/epjc/s10052-021-09280-9](#).
- [66] Ming Zhang and Jie Jiang. Shadows of accelerating black holes. *Phys. Rev. D*, 103(2):025005, 2021. [arXiv:2010.12194](#), [doi:10.1103/PhysRevD.103.025005](#).
- [67] Qingyu Gan, Peng Wang, Houwen Wu, and Haitang Yang. Photon ring and observational appearance of a hairy black hole. *Phys. Rev. D*, 104(4):044049, 2021. [arXiv:2105.11770](#), [doi:10.1103/PhysRevD.104.044049](#).
- [68] Qingyu Gan, Peng Wang, Houwen Wu, and Haitang Yang. Photon spheres and spherical accretion image of a hairy black hole. *Phys. Rev. D*, 104(2):024003, 2021. [arXiv:2104.08703](#), [doi:10.1103/PhysRevD.104.024003](#).
- [69] Subhodeep Sarkar, Shailesh Kumar, and Srijit Bhattacharjee. Can we detect a supertranslated black hole? *Phys. Rev. D*, 105(8):084001, 2022. [arXiv:2110.03547](#), [doi:10.1103/PhysRevD.105.084001](#).
- [70] Merce Guerrero, Gonzalo J. Olmo, Diego Rubiera-Garcia, and Diego Gómez Sáez-Chillón. Light ring images of double photon spheres in black hole and wormhole spacetimes. *Phys. Rev. D*, 105(8):084057, 2022. [arXiv:2202.03809](#), [doi:10.1103/PhysRevD.105.084057](#).
- [71] K. S. Virbhadra. Distortions of images of Schwarzschild lensing. *Phys. Rev. D*, 106(6):064038, 2022.

- [arXiv:2204.01879](#), [doi:10.1103/PhysRevD.106.064038](#). IV
- [72] Sunny Vagnozzi et al. Horizon-scale tests of gravity theories and fundamental physics from the Event Horizon Telescope image of Sagittarius A*. 5 2022. [arXiv:2205.07787](#), [doi:10.1088/1361-6382/acd97b](#).
 - [73] Guangzhou Guo, Xin Jiang, Peng Wang, and Houwen Wu. Gravitational lensing by black holes with multiple photon spheres. *Phys. Rev. D*, 105(12):124064, 2022. [arXiv:2204.13948](#), [doi:10.1103/PhysRevD.105.124064](#).
 - [74] Yiqian Chen, Guangzhou Guo, Peng Wang, Houwen Wu, and Haitang Yang. Appearance of an infalling star in black holes with multiple photon spheres. *Sci. China Phys. Mech. Astron.*, 65(12):120412, 2022. [arXiv:2206.13705](#), [doi:10.1007/s11433-022-1986-x](#).
 - [75] Saptaswa Ghosh and Arpan Bhattacharyya. Analytical study of gravitational lensing in Kerr-Newman black-bounce spacetime. *JCAP*, 11:006, 2022. [arXiv:2206.09954](#), [doi:10.1088/1475-7516/2022/11/006](#). I
 - [76] Abhishek Chowdhuri, Saptaswa Ghosh, and Arpan Bhattacharyya. A review on analytical studies in Gravitational Lensing. *Front. Phys.*, 11:1113909, 2023. [arXiv:2303.02069](#), [doi:10.3389/fphy.2023.1113909](#). I
 - [77] Fabian Schmidt. Weak Lensing Probes of Modified Gravity. *Phys. Rev. D*, 78:043002, 2008. [arXiv:0805.4812](#), [doi:10.1103/PhysRevD.78.043002](#). I
 - [78] Jacek Guzik, Bhuvnesh Jain, and Masahiro Takada. Tests of Gravity from Imaging and Spectroscopic Surveys. *Phys. Rev. D*, 81:023503, 2010. [arXiv:0906.2221](#), [doi:10.1103/PhysRevD.81.023503](#).
 - [79] Kai Liao, Zhengxiang Li, Shuo Cao, Marek Biesiada, Xiaogang Zheng, and Zong-Hong Zhu. The Distance Duality Relation From Strong Gravitational Lensing. *Astrophys. J.*, 822(2):74, 2016. [arXiv:1511.01318](#), [doi:10.3847/0004-637X/822/2/74](#).
 - [80] Prieslei Goulart. Phantom wormholes in Einstein–Maxwell-dilaton theory. *Class. Quant. Grav.*, 35(2):025012, 2018. [arXiv:1708.00935](#), [doi:10.1088/1361-6382/aa9dfc](#).
 - [81] J. R. Nascimento, A. Yu. Petrov, P. J. Porfirio, and A. R. Soares. Gravitational lensing in black-bounce spacetimes. *Phys. Rev. D*, 102(4):044021, 2020. [arXiv:2005.13096](#), [doi:10.1103/PhysRevD.102.044021](#).
 - [82] Xin Qin, Songbai Chen, and Jiliang Jing. Image of a regular phantom compact object and its luminosity under spherical accretions. *Class. Quant. Grav.*, 38(11):115008, 2021. [arXiv:2011.04310](#), [doi:10.1088/1361-6382/abf712](#).
 - [83] Shafqat Ul Islam, Jitendra Kumar, and Sushant G. Ghosh. Strong gravitational lensing by rotating Simpson-Visser black holes. *JCAP*, 10:013, 2021. [arXiv:2104.00696](#), [doi:10.1088/1475-7516/2021/10/013](#).
 - [84] Naoki Tsukamoto. Gravitational lensing by two photon spheres in a black-bounce spacetime in strong deflection limits. 5 2021. [arXiv:2105.14336](#).
 - [85] Haroldo C. D. Lima Junior, Jian-Zhi Yang, Luís C. B. Crispino, Pedro V. P. Cunha, and Carlos

- A. R. Herdeiro. Einstein-Maxwell-dilaton neutral black holes in strong magnetic fields: Topological charge, shadows, and lensing. *Phys. Rev. D*, 105(6):064070, 2022. [arXiv:2112.10802](#), [doi:10.1103/PhysRevD.105.064070](#).
- [86] Gonzalo J. Olmo, Diego Rubiera-Garcia, and Diego Sáez-Chillón Gómez. New light rings from multiple critical curves as observational signatures of black hole mimickers. *Phys. Lett. B*, 829:137045, 2022. [arXiv:2110.10002](#), [doi:10.1016/j.physletb.2022.137045](#). I
- [87] Stuart L. Shapiro and Saul A. Teukolsky. Formation of naked singularities: The violation of cosmic censorship. *Phys. Rev. Lett.*, 66:994–997, 1991. [doi:10.1103/PhysRevLett.66.994](#). I
- [88] P. S. Joshi and I. H. Dwivedi. Naked singularities in spherically symmetric inhomogeneous Tolman-Bondi dust cloud collapse. *Phys. Rev. D*, 47:5357–5369, 1993. [arXiv:gr-qc/9303037](#), [doi:10.1103/PhysRevD.47.5357](#).
- [89] Tomohiro Harada, Hideo Iguchi, and Ken-ichi Nakao. Naked singularity formation in the collapse of a spherical cloud of counter rotating particles. *Phys. Rev. D*, 58:041502, 1998. [arXiv:gr-qc/9805071](#), [doi:10.1103/PhysRevD.58.041502](#).
- [90] Pankaj S. Joshi, Naresh Dadhich, and Roy Maartens. Why do naked singularities form in gravitational collapse? *Phys. Rev. D*, 65:101501, 2002. [arXiv:gr-qc/0109051](#), [doi:10.1103/PhysRevD.65.101501](#).
- [91] Rituparno Goswami and Pankaj S Joshi. Spherical gravitational collapse in N-dimensions. *Phys. Rev. D*, 76:084026, 2007. [arXiv:gr-qc/0608136](#), [doi:10.1103/PhysRevD.76.084026](#).
- [92] Narayan Banerjee and Soumya Chakrabarti. Self-similar scalar field collapse. *Phys. Rev. D*, 95(2):024015, 2017. [arXiv:1701.04235](#), [doi:10.1103/PhysRevD.95.024015](#).
- [93] Kaushik Bhattacharya, Dipanjan Dey, Arindam Mazumdar, and Tapobrata Sarkar. New class of naked singularities and their observational signatures. *Phys. Rev. D*, 101(4):043005, 2020. [arXiv:1709.03798](#), [doi:10.1103/PhysRevD.101.043005](#). I
- [94] K. S. Virbhadra and G. F. R. Ellis. Gravitational lensing by naked singularities. *Phys. Rev. D*, 65:103004, 2002. [doi:10.1103/PhysRevD.65.103004](#). I
- [95] K. S. Virbhadra and C. R. Keeton. Time delay and magnification centroid due to gravitational lensing by black holes and naked singularities. *Phys. Rev. D*, 77:124014, 2008. [arXiv:0710.2333](#), [doi:10.1103/PhysRevD.77.124014](#).
- [96] Galin N. Gyulchev and Stoytcho S. Yazadjiev. Gravitational Lensing by Rotating Naked Singularities. *Phys. Rev. D*, 78:083004, 2008. [arXiv:0806.3289](#), [doi:10.1103/PhysRevD.78.083004](#). I
- [97] Satyabrata Sahu, Mandar Patil, D. Narasimha, and Pankaj S. Joshi. Can strong gravitational lensing distinguish naked singularities from black holes? *Phys. Rev. D*, 86:063010, 2012. [arXiv:1206.3077](#), [doi:10.1103/PhysRevD.86.063010](#).
- [98] Rajibul Shaikh, Pritam Banerjee, Suvankar Paul, and Tapobrata Sarkar. Analytical approach to strong gravitational lensing from ultracompact objects. *Phys. Rev. D*, 99(10):104040, 2019. [arXiv:1903.08211](#), [doi:10.1103/PhysRevD.99.104040](#).

- [99] Suvankar Paul. Strong gravitational lensing by a strongly naked null singularity. *Phys. Rev. D*, 102(6):064045, 2020. [arXiv:2007.05509](#), [doi:10.1103/PhysRevD.102.064045](#).
- [100] Naoki Tsukamoto. Gravitational lensing by a photon sphere in a Reissner-Nordström naked singularity spacetime in strong deflection limits. *Phys. Rev. D*, 104(12):124016, 2021. [arXiv:2107.07146](#), [doi:10.1103/PhysRevD.104.124016](#).
- [101] Mingzhi Wang, Guanghai Guo, Pengfei Yan, Songbai Chen, and Jiliang Jing. The images of a rotating naked singularity with a complete photon sphere. 7 2023. [arXiv:2307.16748](#).
- [102] Yiqian Chen, Peng Wang, Houwen Wu, and Haitang Yang. Gravitational Lensing by Born-Infeld Naked Singularities. 5 2023. [arXiv:2305.17411](#). I, III, IV B
- [103] Rajibul Shaikh, Prashant Kocherlakota, Ramesh Narayan, and Pankaj S. Joshi. Shadows of spherically symmetric black holes and naked singularities. *Mon. Not. Roy. Astron. Soc.*, 482(1):52–64, 2019. [arXiv:1802.08060](#), [doi:10.1093/mnras/sty2624](#). I
- [104] Allen I. Janis, Ezra T. Newman, and Jeffrey Winicour. Reality of the Schwarzschild Singularity. *Phys. Rev. Lett.*, 20:878–880, 1968. [doi:10.1103/PhysRevLett.20.878](#). I, II A, II A
- [105] K. S. Virbhadra, D. Narasimha, and S. M. Chitre. Role of the scalar field in gravitational lensing. *Astron. Astrophys.*, 337:1–8, 1998. [arXiv:astro-ph/9801174](#). I
- [106] Anirban N. Chowdhury, Mandar Patil, Daniele Malafarina, and Pankaj S. Joshi. Circular geodesics and accretion disks in Janis-Newman-Winicour and Gamma metric. *Phys. Rev. D*, 85:104031, 2012. [arXiv:1112.2522](#), [doi:10.1103/PhysRevD.85.104031](#).
- [107] Galin Gyulchev, Petya Nedkova, Tsvetan Vetsov, and Stoytcho Yazadjiev. Image of the Janis-Newman-Winicour naked singularity with a thin accretion disk. *Phys. Rev. D*, 100(2):024055, 2019. [arXiv:1905.05273](#), [doi:10.1103/PhysRevD.100.024055](#).
- [108] Subhadip Sau, Indrani Banerjee, and Soumitra SenGupta. Imprints of the Janis-Newman-Winicour spacetime on observations related to shadow and accretion. *Phys. Rev. D*, 102(6):064027, 2020. [arXiv:2004.02840](#), [doi:10.1103/PhysRevD.102.064027](#).
- [109] Cristian Martinez and Masato Nozawa. Static spacetimes haunted by a phantom scalar field. I. Classification and global structure in the massless case. *Phys. Rev. D*, 103(2):024003, 2021. [arXiv:2010.05183](#), [doi:10.1103/PhysRevD.103.024003](#).
- [110] Divyesh N. Solanki, Parth Bambhaniya, Dipanjan Dey, Pankaj S. Joshi, and Kamlesh N. Pathak. Shadows and precession of orbits in rotating Janis–Newman–Winicour spacetime. *Eur. Phys. J. C*, 82(1):77, 2022. [arXiv:2109.14937](#), [doi:10.1140/epjc/s10052-022-10045-1](#).
- [111] Bertrand Chauvineau. Lensing by a Fisher-Janis-Newman-Winicour naked singularity: Observational issues related to the existence of caustic bending in the strongly scalarized case. *Phys. Rev. D*, 105(2):024071, 2022. [Erratum: Phys.Rev.D 106, 129901 (2022)]. [doi:10.1103/PhysRevD.105.024071](#).
- [112] Alireza Azizollahi, Behrouz Mirza, Arash Hajibarat, and Homayon Anjomshoa. Three parameter metrics in the presence of a scalar field in four and higher dimensions. 7 2023. [arXiv:2307.09328](#). I

- [113] K. S. Virbhadra, S. Jhingan, and P. S. Joshi. Nature of singularity in Einstein massless scalar theory. *Int. J. Mod. Phys. D*, 6:357–362, 1997. [arXiv:gr-qc/9512030](#), [doi:10.1142/S0218271897000200](#). II A
- [114] Kunal Pal, Kuntal Pal, Pratim Roy, and Tapobrata Sarkar. Regularizing the JNW and JMN naked singularities. *Eur. Phys. J. C*, 83(5):397, 2023. [arXiv:2206.11764](#), [doi:10.1140/epjc/s10052-023-11558-z](#). II C
- [115] Peng Wang, Houwen Wu, Haitang Yang, and Shuxuan Ying. Non-singular string cosmology via α' corrections. *JHEP*, 10:263, 2019. [arXiv:1909.00830](#), [doi:10.1007/JHEP10\(2019\)263](#). II C
- [116] Peng Wang, Houwen Wu, Haitang Yang, and Shuxuan Ying. Construct α' corrected or loop corrected solutions without curvature singularities. *JHEP*, 01:164, 2020. [arXiv:1910.05808](#), [doi:10.1007/JHEP01\(2020\)164](#).
- [117] Shuxuan Ying. Resolving naked singularities in α' -corrected string theory. *Eur. Phys. J. C*, 82(6):523, 2022. [arXiv:2112.03087](#), [doi:10.1140/epjc/s10052-022-10427-5](#). II C
- [118] Xiaobao Wang, Peng-Cheng Li, Cheng-Yong Zhang, and Minyong Guo. Novel shadows from the asymmetric thin-shell wormhole. *Phys. Lett. B*, 811:135930, 2020. [arXiv:2007.03327](#), [doi:10.1016/j.physletb.2020.135930](#). II C
- [119] Yiqian Chen, Peng Wang, Houwen Wu, and Haitang Yang. Observational appearance of a freely-falling star in an asymmetric thin-shell wormhole. *Eur. Phys. J. C*, 83(5):361, 2023. [arXiv:2210.10948](#), [doi:10.1140/epjc/s10052-023-11486-y](#). II C
- [120] Silvia Mollerach and Esteban Roulet. *Gravitational lensing and microlensing*. World Scientific, 2002. IV, IV
- [121] V. Bozza. Gravitational lensing in the strong field limit. *Phys. Rev. D*, 66:103001, 2002. [arXiv:gr-qc/0208075](#), [doi:10.1103/PhysRevD.66.103001](#). IV A, IV A
- [122] Naoki Tsukamoto. Deflection angle in the strong deflection limit in a general asymptotically flat, static, spherically symmetric spacetime. *Phys. Rev. D*, 95(6):064035, 2017. [arXiv:1612.08251](#), [doi:10.1103/PhysRevD.95.064035](#). IV A
- [123] Michael D. Johnson et al. Universal interferometric signatures of a black hole’s photon ring. *Sci. Adv.*, 6(12):eaaz1310, 2020. [arXiv:1907.04329](#), [doi:10.1126/sciadv.aaz1310](#). V
- [124] Elizabeth Himwich, Michael D. Johnson, Alexandru Lupsasca, and Andrew Strominger. Universal polarimetric signatures of the black hole photon ring. *Phys. Rev. D*, 101(8):084020, 2020. [arXiv:2001.08750](#), [doi:10.1103/PhysRevD.101.084020](#).
- [125] Samuel E. Gralla, Alexandru Lupsasca, and Daniel P. Marrone. The shape of the black hole photon ring: A precise test of strong-field general relativity. *Phys. Rev. D*, 102(12):124004, 2020. [arXiv:2008.03879](#), [doi:10.1103/PhysRevD.102.124004](#). V